COUPLED HYDRO-THERMAL-MECHANICAL ANALYSIS FOR COLD CO_2 INJECTION INTO A DEEP SALINE AQUIFER

by

Huimin WANG [a,c], ***Jianguo WANG*** [a,b*], ***and Xiaolin WANG*** [c], ***Fakai DOU*** [a], ***and Bowen HU*** [b]

[a] State Key Laboratory for GeoMechanics and Deep Underground Engineering, China University of Mining and Technology, Xuzhou, China
[b] School of Mechanics and Civil Engineering, China University of Mining and Technology, Xuzhou, China
[c] School of Engineering, University of Tasmania, Hobart, Tasmania, Australia

Original scientific paper
https://doi.org/10.2298/TSCI180511127W

This study investigated the thermal effects of thermal stress and Joule-Thomson cooling on CO_2 migration in a deep saline aquifer through a hydro-thermal-mechanical model. Firstly, the temperature variation of injected CO_2 was analyzed through the coupling of two-phase flow, deformation of porous medium and heat transfer with Joule-Thomson effect. Then, the effect of capillary entry pressure on CO_2 plume was numerically investigated and compared. It is found that injection temperature and Joule-Thomson effect can significantly affect the distributions of CO_2 mass and temperature, particularly in the upper zone near the injection well. The reduction of capillary entry pressure accelerates the upward migration of CO_2 plume and increases the CO_2 lateral migration distance.

Key words: *CO_2 storage, two-phase flow, Joule-Thomson effect, thermal stress, multi-physical process*

Introduction

Carbon capture and storage (CCS) has become one of the most effective choices to reduce CO_2 emissions [1, 2]. Deep geological aquifers were widely used as CO_2 storage reservoirs [3]. The long-term sequestration of CO_2 in the reservoir is safeguarded by the sealing efficiency of overlying caprocks. The behavior of CO_2 flow in the storage reservoirs is the first step to the success of CO_2 sequestration [4]. Current analysis for the first step usually assumes a constant temperature of reservoir (called isothermal process later). In this isothermal process, the physical properties (density and viscosity) of CO_2 do not change with temperature. However, heat transfer is a complex process with strong non-linearity [5, 6]. Such an assumption of isothermal process may affect the prediction accuracy of CO_2 flow behavior.

Injected CO_2 is usually colder than the reservoir. This causes thermal contraction and thermal stress [7, 8]. When high pressure CO_2 is injected into the low pressure reservoir, the CO_2 expands, causing further temperature drop due to Joule-Thomson cooling. Vilarrasa *et al.* [9] compared the flow behaviors of liquid CO_2 and supercritical CO_2 in the reservoir. They found that the injection efficiency of liquid CO_2 is higher due to higher density of liquid CO_2 and smaller resultant over pressure. This indicates that the change of CO_2 physical properties

* Corresponding author, e-mail: jgwang@cumt.edu.cn, nuswjg@yahoo.com

during injection is indeed worth of multi-physical modelling. Mathias *et al*. [10] developed a simple analytical solution and found that Joule-Thomson cooling is a negative factor for CO_2 storage. In this solution, the permeability of reservoir is constant and the accumulation of pore pressure and the thermal stress were not considered. Gao *et al*. [11] proposed traveling-wave solutions for both linear and non-linear heat transfers. They only considered the temperature variation without the thermal-mechanical coupling. This is not enough to understand the CO_2 flow behavior in the geological storage. Gor *et al*. [12] established a multi-phase model to investigate the effect of thermal stress on caprock integrity. Their simulations showed that the stress above the horizontal injection well may lead to tensile or shear failure of the caprock. Kim *et al*. [7] conducted a numerical simulation include fluid-flow, thermal stress and thermal diffusion. However, their simulation was based on single-phase flow. The effects of relative permeability parameters on CO_2 migration in the reservoir have not been included. The above studies have demonstrated the importance of non-isothermal flow of CO_2 in a deep saline aquifer, but a coupled hydro-thermal-mechanical model is still missing.

This study will extend our previous two-phase flow model [13] to include the thermal stress and Joule-Thomson effects. Thermal stress is included in a new porosity model to investigate the matrix shrinkage caused by cold CO_2 injection. The Joule-Thomson effect is considered in the changes of CO_2 physical properties. Further, the effect of capillary entry pressure on CO_2 migration is also included in the model.

Governing equations for non-isothermal two-phase flow

Mass conservation equation for two-phase flow

The mass conservation laws for the flow of water and CO_2 in porous medium are [14, 15]:

$$\frac{\partial(\phi\rho_{\mathrm{w}}s_{\mathrm{w}})}{\partial t}+\nabla\left[-\frac{kk_{\mathrm{rw}}}{\mu_{\mathrm{w}}}\rho_{\mathrm{w}}(\nabla p_{\mathrm{w}}+\rho_{\mathrm{w}}\mathrm{g}\nabla H)\right]=Q_{\mathrm{w}} \tag{1}$$

$$\frac{\partial m}{\partial t}+\nabla\left[-\frac{kk_{\mathrm{rg}}}{\mu_{\mathrm{g}}}\rho_{\mathrm{g}}(\nabla p_{\mathrm{g}}+\rho_{\mathrm{g}}\mathrm{g}\,\nabla H)\right]=Q_{\mathrm{g}} \tag{2}$$

and

$$m=\phi\rho_{\mathrm{g}}s_{\mathrm{g}}+\rho_{\mathrm{ga}}\rho_{\mathrm{c}}\frac{V_{\mathrm{L}}p_{\mathrm{g}}}{p_{\mathrm{L}}+p_{\mathrm{g}}}\exp\left(-\frac{c_1\Delta T}{1+c_2p_{\mathrm{g}}}\right) \tag{3}$$

where ϕ is the porosity, s_{w} – the saturation of water, p_{w} – the water pressure, p_{g} – the gas pressure, ρ_{w} – the density of water, ρ_{g} – the density of CO_2, k – the intrinsic permeability, k_{rw} – the relative permeability of water, k_{rg} – the relative permeability of gas, μ_{w} – the viscosity of water, μ_{g} – the viscosity of gas, g – the gravitational acceleration, H – the elevation in vertical direction, Q_{w} – the source of water, Q_{g} – the source of CO_2, s_{g} – the saturation of CO_2, ρ_{c} – the density of rock, ρ_{ga} – the CO_2 density under the standard conditions, V_{L} – the Langmuir volume constant, p_{L} – the Langmuir pressure, c_1 [K^{-1}] – the temperature correction coefficient of gas adsorption, and c_2 [MPa^{-1}] – the pressure correction coefficient of gas adsorption.

The density of CO_2:

$$\rho_{\mathrm{g}}=\frac{M_{\mathrm{CO_2}}}{ZRT}p_{\mathrm{g}} \tag{4}$$

where M_{CO2} is the molecular weight of CO_2, R – the universal gas constant, T – the gas temperature, and Z – the compressibility factor of real gas.

Since the pressure and the temperature of CO_2 in this study vary in a certain range (14MPa-26MPa 310K-324K). The compressibility factor Z can be defined as an interpolation factor for the computation in Comsol Multiphysics. The compressibility with respect to temperature and pressure can be derived:

$$c_T = \frac{1}{\rho_g}\frac{\partial \rho_g}{\partial T} = -\left(\frac{1}{T} + \frac{1}{Z}\frac{\partial Z}{\partial T}\right) \tag{5}$$

and

$$= \frac{1}{g}\frac{\partial}{\partial p_g} = \left(\frac{1}{p_g} - \frac{1}{Z}\frac{\partial}{p_g}\right) \tag{6}$$

Heidaryan *et al*. [16] developed a formula to calculate the CO_2 viscosity in ranges of pressure (7.5-101.4 MPa) and temperature (310-900 K):

$$\mu_g = \frac{A_1 + A_2 + A_3 p_g^2 + A_4 \ln(T) + A_5[\ln(t)]^2 + A_6[\ln(t)]^3}{1 + A_7 p_g + A_8 \ln(T) + A_9[\ln(t)]^2} \tag{7}$$

where the pressure and the temperature are expressed in bar and K, respectively. The viscosity unit is centipoise, c_p. Unit conversion is required before calculation. The A_1-A_9 are the tuned coefficients [16]. Substituting eqs. (3)-(6) into eqs. (1) and (2) obtains the final governing equations of two-phase flow:

$$\phi c_s \frac{\partial p_g}{\partial t} - \phi c_s \frac{\partial p_w}{\partial t} + \nabla\left[-\frac{kk_{rw}}{\mu_w}(\nabla p_w + \rho_w g \nabla H)\right] = Q_w' - s_w \frac{\partial \phi}{\partial t} \tag{8}$$

$$\left[-\phi c_s + \phi s_g c_p + \frac{\rho_{ga}\rho_c}{\rho_g}\exp\left(-\frac{c_1 \Delta T}{1 + c_2 p_g}\right)\left(\frac{V_L P_L}{(P_L + p_g)^2} - \frac{V_L p_g}{P_L + p_g}\frac{c_1 c_2 \Delta T}{(1 + c_2 p_g)^2}\right)\right]\frac{\partial p_g}{\partial t} + \phi c_s \frac{\partial p_w}{\partial t} +$$

$$+\nabla\left[-\frac{kk_{rg}}{\mu_g}(\nabla p_g + \rho_g g \nabla H)\right] = -\left[\phi s_g c_T \frac{\rho_{ga}\rho_c}{\rho_g}\frac{V_L p_g}{P_L + p_g}\exp\left(-\frac{c_1 \Delta T}{1 + c_2 p_g}\right)\frac{-c_1}{1 + c_2 p_g}\right]\frac{\partial T}{\partial t} - s_g \frac{\partial \phi}{\partial t} + Q_g' \tag{9}$$

where c_s is the compressibility with respect to capillary pressure, which is obtained from the relationship of water saturation and capillary pressure. The detail of c_s can refer to our previous work [14, 15]. The $Q_w = \rho_w Q'_w$ and $Q_g = \beta Q'_g$, β *i*s a constant.

Thermoelastic strain in porous media

The porosity model considering both thermal strain and sorption strain is proposed:

$$\phi = \phi_0 + \alpha\left(\varepsilon_v + \frac{p}{K_s} - \varepsilon_{s1} - \varepsilon_{s2}\right) \tag{10}$$

where ϕ_0 – the initial porosity, ϕ – the current porosity, α – the Biot coefficient, K_s – the bulk modulus of rock grain, p – the gas pressure in pores, ε_v – the volumetric strain, ε_{s1} – the sorption strain, and ε_{s2} – the thermal strain.

The evolution of porosity in the two-phase flow is further expressed:

$$\frac{\partial \phi}{\partial t} = \alpha\left(\frac{\partial \varepsilon_v}{\partial t} + \frac{1}{K_s}\frac{\partial p}{\partial t} - \frac{\partial \varepsilon_{s1}}{\partial t} - \alpha_T \frac{\partial T}{\partial t}\right) \tag{11}$$

Energy conservation for heat transfer

During the injection of CO_2 into the geological reservoir, the heat transfer satisfies the energy conservation [17, 18]:

$$\frac{\partial(C_{eq}T)}{\partial t}-\phi(\rho_g C_g \mu_{JT}+1)\frac{\partial p_g}{\partial t}+K\alpha_T T\frac{\partial \varepsilon_v}{\partial t}+\nabla v_T=0 \tag{12}$$

where K is the bulk modulus of porous media, α_T – the thermal expansion coefficient, and μ_{JT} is the Joule-Thomson coefficient, $C_{eq}=\phi\rho_g C_g+(1-\phi)\rho_c C_s$ – the specific heat capacity of porous medium, and v_T – the represents average heat transfer rate and can be divided into heat conduction and heat convection:

$$v_T=-K_{eq}\nabla T+\rho_g C_g\frac{kk_{rg}}{\mu_g}\nabla p_g(T-\mu_{JT}p_g) \tag{13}$$

where K_{eq} is the thermal conductivity, C_g – the specific heat capacity of CO_2, and C_s – the specific heat capacity of rock.

Substituting eq. (13) into eq. (12) gets the final governing equation of heat transfer:

$$[\phi\rho_g C_g+(1-\phi)\rho_c C_s)\frac{\partial T}{\partial t}-\phi(\rho_g C_g\mu_{JT}+1)\frac{\partial p_g}{\partial t}+K\alpha_T T\frac{\partial \varepsilon_v}{\partial t}=$$
$$=K_{eq}\nabla^2 T+\rho_g C_g\frac{kk_{rg}}{\mu_g}\nabla p_g(\nabla T-\mu_{JT}\nabla p_g) \tag{14}$$

Set-up of numerical model

The same geological formation was used by Vilarrasa *et al*. [9]. We have studied the penetration of CO_2 into the caprock in our previous study [14], thus this study only focuses on the non-isothermal flow of CO_2 in the storage reservoir. As shown in fig. 1, the computational model is composed of a 2-D domain and is located at the depth of 1500 m. The domain is 1000 m long and 100 m high. Its top and bottom boundaries are no-flow. The hydrostatic pressure is initially distributed in the computational domain as initial reservoir pressure. The reservoir temperature is 322.5 K. The cold CO_2 (310 K, still in supercritical state) is injected from the left boundary with a prescribed CO_2 mass flow rate (1.0 Mt per year). The model parameters are listed in tab. 1.

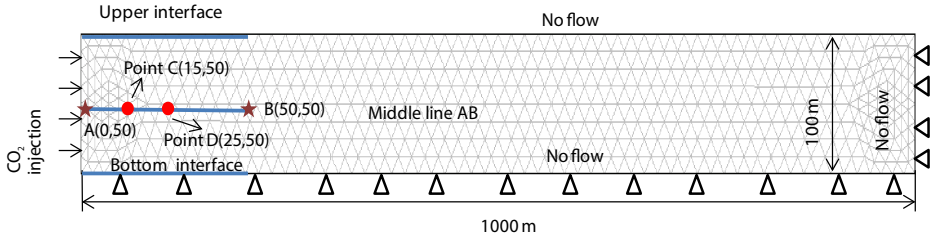

Figure 1. A 2-D computational model

Results and discussions

Temperature evolution near the injection well

When a large amount of cold CO_2 is injected into the reservoir, the profile of temperature will change with heat transfer, especially near the injection well. Figure 2 is the tempera-

Table 1. Model parameters used in computation

Parameter	Unit	Value	Physical meanings
μ_w	[Pa·s]	$5.5 \cdot 10^{-4}$	Water viscosity
p_{w0}	[MPa]	$10.1 + 0.0102(500 - y)$	Initial water pressure in reservoir
p_{g0}	[MPa]	$p_{w0} + p_e$	Initial CO_2 pressure in reservoir
p_e	[MPa]	0.1	Capillary entry pressure
T_0	[K]	323	Temperature
k_0	[m^2]	$1 \cdot 10^{-13}$	Initial absolute permeability
ϕ_0		0.15	Initial porosity
ν		0.25	Poisson's ratio of shale
ρ_c	[kgm^{-3}]	1250	Shale density
P_L	[MPa]	6	Langmuir pressure
V_L	[m^3kg^{-1}]	0.03	Langmuir sorption capacity
ε_L		0.015	Langmuir swelling strain
ρ_w	[kgm^{-3}]	1020	Water density
C_g	[$Jkg^{-1}K^{-1}$]	800	Specific heat of CO_2
C_s	[$Jkg^{-1}K^{-1}$]	900	Specific heat of rock
α_T	[K^{-1}]	$1 \cdot 10^{-5}$	Coefficient of thermal expansion
μ_{JT}	[$KMPa^{-1}$]	0.7	Joule-Thomson coefficient

ture distribution along the AB line after 1 month, 6 months, and 1 year of CO_2 injection. After 1 month of CO_2 injection, the temperature influence range is less than 10 m. After one year, the range is expanded to 50 m away from the injection well. These results indicate that the cold CO_2 injection only affects the temperature in the zone near the injection well. The CO_2 will be in equilibrium with reservoir temperature in a short range of injection well.

Since CO_2 migrates upward under buoyancy, the temperature transfer also shows the coincidence with gas-flow. The upper, middle and bottom lines are displayed in the computational model. Figure 3 shows the distribution of temperature along these three lines after one year of CO_2 injection. Temperature changes are almost the same along the middle and bottom boundaries. However, the temperature distribution at the upper boundary is significantly lower than other two lines. This also indicates that the upward migration of CO_2 causes the temperature decrease in the upper area of the reservoir.

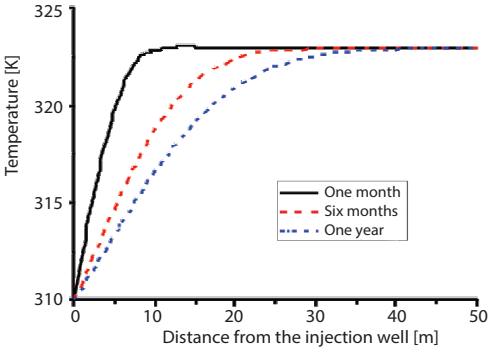

Figure 2. Distribution of CO_2 temperature near the well

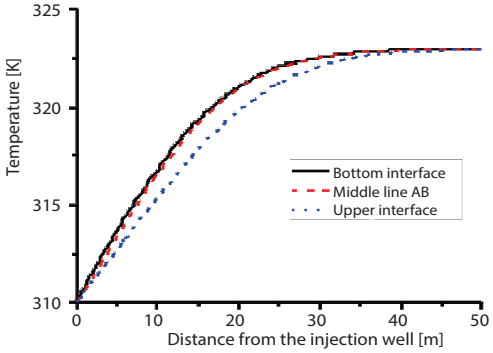

Figure 3. Temperature distribution along three horizontal lines at one-year CO_2 injection

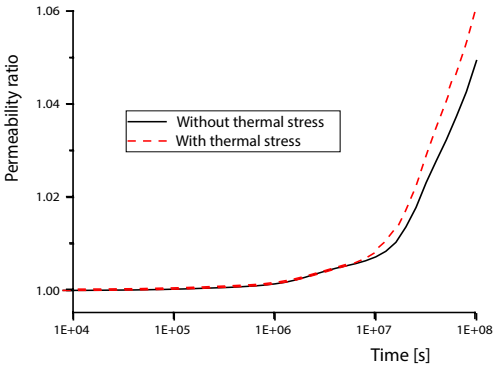

Figure 4. Comparison of permeability ratio at point C (15.50) with /without thermal stress

Thermal stress causes the change of permeability in this hydro-thermal-mechanical coupled model. The flow of cold CO_2 brings a cooling effect to the reservoir, so the matrix shrinks and the permeability increases. Figure 4 shows the comparison of permeability ratio at a typical point C (15.50) with and without thermal stress. Since the injection of CO_2 causes an increase in pore pressure, more pore space is opened. The permeability increases whether the flow is isothermal or non-isothermal. However, the permeability increases more at the non-isothermal flow due to thermal stress. This increase of permeability makes CO_2 migrate more easily.

Effect of Joule-Thomson cooling on CO_2 physical properties

A great pressure drop would occur near the well when CO_2 is injected into the reservoir. Due to the Joule-Thomson effect, this pressure drop can also give rise to a temperature drop. The physical properties of CO_2 (density and viscosity) experience a significant change near the injection well due to the combination action of temperature and pressure drops. The density directly affects the storage efficiency of CO_2 in the reservoir. The viscosity is related to the CO_2 migration in the reservoir and the pressure buildup at the bottom of the caprock. Figure 5 shows the distributions of CO_2 saturation with or without Joule-Thomson effect after one-year injection. Because the constitutive relationship between saturation and capillary pressure is the same, the front of CO_2 displacing water is almost identical. However, with considering the Joule-Thomson effect, the injected high pressure CO_2 expands freely and the density decreases. More CO_2 migrates upward under the action of buoyancy. Thus, this CO_2 saturation is higher.

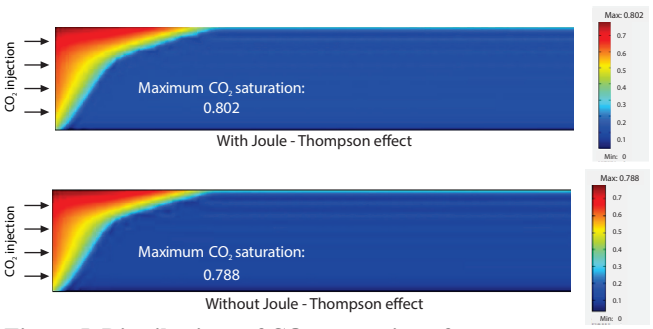

Figure 5. Distributions of CO_2 saturation after one-year injection

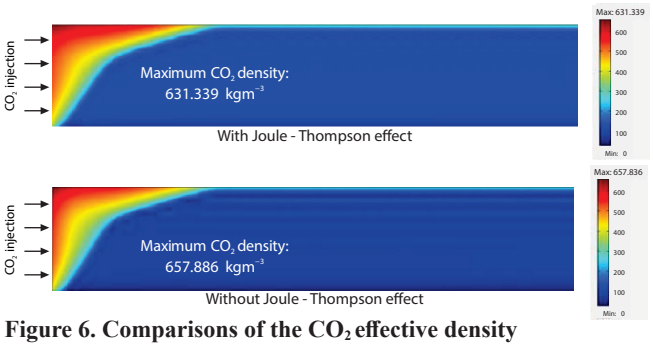

Figure 6. Comparisons of the CO_2 effective density after one-year injection

In order to evaluate this injection efficiency, we define the effective density of CO_2 ($\rho_e = s_g\rho_g$). Figure 6 gives the comparison of effective density. The CO_2 saturation is higher after considering the Joule-Thomson effect in fig. 5, but the effective density is lower. This implies that

Joule-Thomson effect reduces the injection efficiency of CO_2.

The viscosity of CO_2 is an important parameter related to flow mobility. The viscosity increases with the accumulation of pressure when high pressure CO_2 is injected into the reservoir. When the CO_2 injection pressure remains the same, the variations of injection temperature become more important to the CO_2 viscosity. Figure 7 shows the evolutions of CO_2 viscosity with injection temperature of 310 K, 314 K, and 318 K. The injected CO_2 is colder, the viscosity is higher. This increase of viscosity makes CO_2 migrate slower in the reservoir.

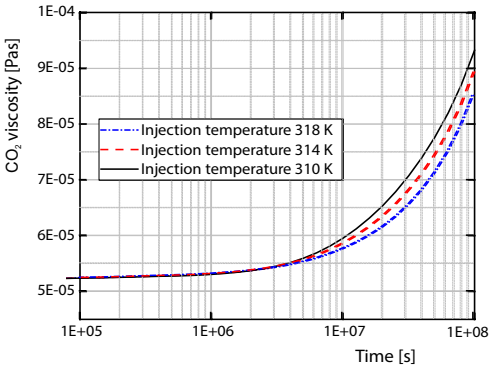

Figure 7. Variation of CO_2 viscosity at point D (25, 50) under different injection temperatures

Effect of capillary entry pressure on CO_2 plume

Capillary entry pressure does not only determine the efficiency of CO_2 capillary capture, but also affects the degree of CO_2 displacing water in the caprock. The capillary entry pressure has a wide variation from 0.1-48.3 MPa. This value depends on different geological reservoir or caprock. In this study, the capillary entry pressure is assumed to be 0.1, 0.2, and 0.3 MPa, respectively.

Figure 8 shows the spatial distribution of CO_2 plume after three years of CO_2 injection. When the capillary entry pressure is 0.1 MPa, the injected CO_2 firstly migrates upward under the action of buoyancy, and quickly accumulates at the bottom of the caprock and migrates laterally. As the capillary pressure increases, the lateral migration distance of the CO_2 plume is significantly reduced. This implies that capillary entry pressure prevents the spatial migration of CO_2. In addition, the increase of capillary entry pressure causes the increase of CO_2 capillary storage efficiency. It is found that more CO_2 is sealed in the zone near the injection well instead of migrating upwards.

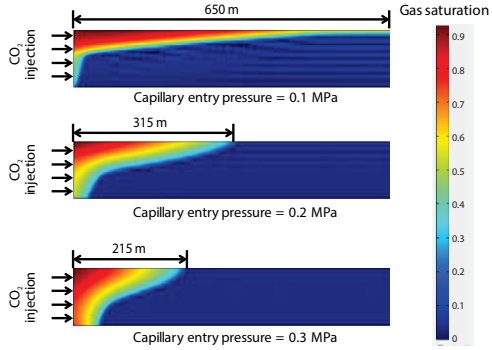

Figure 8. Effect of capillary entry pressure on the shape of CO_2 plume after three year injection

The migration distance of CO_2 in the lateral direction is related to the accumulation of gas pressure under the caprock. This is important to the CO_2 storage efficiency in the reservoir and will further affect the stability of the caprock in a longer time. Thus, we calculate the lateral migration distance of CO_2 after three year injection when the capillary entry pressure is 0.1, 0.15, 0.2, 0.25, and 0.3 MPa, respectively. The results

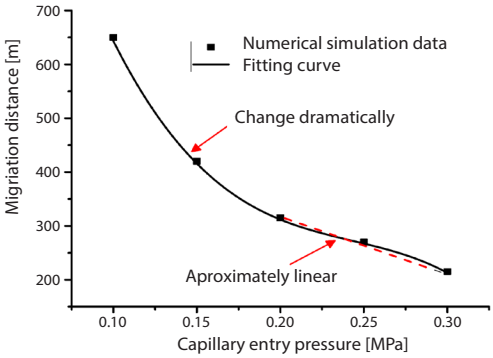

Figure 9. The CO_2 migration distance varies with capillary entry pressure

are presented in fig. 9. With the increase of capillary entry pressure, the lateral migration distance of CO_2 decreases significantly. Especially when the capillary entry pressure is below 0.2 MPa, the lateral migration distance changes dramatically. As the capillary entry pressure increases, a linear relationship with the lateral migration distance is approximately observed. This indicates that capillary entry pressure is an important parameter to the CO_2 storage efficiency.

Conclusion

This study extends our previous two-phase flow model to include the thermal effects (thermal stress and Joule-Thomson cooling). The following conclusions can be drawn: the temperature effect of cold CO_2 mainly occurs near the injection well, and the temperature of the upper interface is lower due to the CO_2 upward migration. The permeability ratio of non-isothermal flow is 1.1% higher than that of isothermal flow due to thermal stress. The density of CO_2 decreases slightly with considering the Joule-Thomson effect. The injected CO_2 temperature is lower, and the viscosity is greater, capillary entry pressure affects the shape of CO_2 plume. When capillary entry pressure is lower, more CO_2 migrates upward under buoyancy and the CO_2 lateral migration distance is greater.

Acknowledgment

The authors are grateful to the financial support from the National Natural Science Foundation of China (Grant No. 51674246) and the State Key Research Development Program of China (2016YFC0600705).

References

[1] Johnsson, F., *et al*.,The Importance of CO_2 Capture and Storage: A Geopolitical Discussion, *Thermal Science*, *16* (2012), 3, pp. 655-668
[2] Li, C., *et al*., Coupled Multi-Phase Thermo-Hydro-Mechanical Analysis of Supercritical CO_2 Injection: Benchmark for the in Salah Surface Uplift Problem, *International Journal of Greenhouse Gas Control*, *51* (2016), Aug., pp. 394-408
[3] Wei, X., *et al*., Modelling the Hydro Mechanical Responses of Sandwich Structure Faults during under Ground Fluid Injection, *Environmental Earth Sciences*, *75* (2016), 16, pp. 1155-1170
[4] Mijic, A., *et al*., The CO_2 Injectivity in Saline Aquifers: the Impact of non-Darcy Flow, Phase Miscibility, and Gas Compressibility, *Water Resources Research*, *50* (2014), 5, pp. 4163-4185
[5] Yang, X. J., *et al*., Some New Applications for Heat and Fluid-flows via Fractional Derivatives without Singular Kernel, *Thermal Science*, *20* (2016), Suppl. 3, pp. S833-S839
[6] Yang, X. J., *et al*., A New Technology for Solving Diffusion and Heat Equations, *Thermal Science*, *21* (2017), 1A, pp. 133-140
[7] Kim, S., *et al.*, Hydro-Thermo-Mechanical Analysis During Injection of Cold Fluid into a Geologic Formation, *International Journal of Rock Mechanics and Mining Sciences, 77* (2015), 4, pp. 220-236
[8] Vilarrasa, V., *et al.*,Thermal and Capillary Effects on the Caprock Mechanical Stability at In Salah, Algeria, *Greenhouse Gases Science & Technology, 5* (2015), 4, pp. 449-461
[9] Vilarrasa, V., *et al.*, Liquid CO_2 Injection for Geological Storage in Deep Saline Aquifers, *International Journal of Greenhouse Gas Control, 14* (2013), 14, pp. 84-96
[10] Mathias, S. A., *et al*., Analytical Solution for Joule-Thomson Cooling during CO_2 Geo-Sequestration in Depleted Oil and Gas Reservoirs, *International Journal of Greenhouse Gas Control*, *4* (2010), 5, pp. 806-810
[11] Gao, F., *et al*., Exact Traveling-Wave Solutions for Linear and Non-linear Heat Transfer Equations, *Thermal Science*, *21* (2017), 4, pp. 321-321
[12] Gor, G., *et al*., Effects of Thermal Stresses on Caprock Integrity during CO_2 Storage, *International Journal of Greenhouse Gas Control*, *12* (2013), 1, pp. 300-309
[13] Wang, H., *et al.*, A Two-Phase Flowback Model for Multiscale Diffusion and Flow in Fractured Shale Gas Reservoirs, *Geofluids*, *2018* (2018), June, ID 5910437

[14] Wang, J. G., *et al*., Numerical Modelling for the Combined Effects of Two-Phase Flow, Deformation, Gas Diffusion and CO_2, Sorption on Caprock Sealing Efficiency, *Journal of Geochemical Exploration*, *144* (2014), Part A, pp. 154-167
[15] Wang, J. G., *et al*., Effect of CO_2 Sorption-Induced Anisotropic Swelling on Caprock Sealing Efficiency, *Journal of Cleaner Production*, *103* (2015), Sept., pp. 685-695
[16] Heidaryan, E., *et al*., Viscosity of Pure Carbon Dioxide at Supercritical Region: Measurement and Correlation Approach, *Journal of Supercritical Fluids*, *56* (2011), 2, pp. 144-151
[17] Ziabakhsh-Ganji, Z., *et al*., Sensitivity of Joule-Thomson Cooling to Impure CO_2 Injection in Depleted Gas Reservoirs, *Applied Energy*, *113* (2014), 6, pp. 434-451
[18] Teng, T., *et al*., Complex Thermal Coal-Gas Interactions in Heat Injection Enhanced CBM Recovery, *Journal of Natural Gas Science and Engineering*, *34* (2016), Aug., pp. 1174-1190

Paper submitted: May 11, 2018
Paper revised: June 21, 2018
Paper accepted: November 15, 2018